Development of templated RuO2 nanorod and nanosheet electrodes to improve the electrocatalytic activities for chlorine evolution

Article · October 2017

DOI: 10.11001/jksww.2017.31.5.373

CITATIONS
0

READS
141

3 authors, including:

Tran Le Luu
Vietnamese German Univerity
19 PUBLICATIONS **85** CITATIONS

SEE PROFILE

Choonsoo Kim
Kongju National University
47 PUBLICATIONS **1,144** CITATIONS

SEE PROFILE

ISSN(Print): 1225-7672 / ISSN(Online): 2287-822X
DOI https://doi.org/10.11001/jksww.2017.31.5.373

Development of templated RuO_2 nanorod and nanosheet electrodes to improve the electrocatalytic activities for chlorine evolution

전기적 염소 발생 촉매활성을 위한 성형된 루테늄 산화물 나노로드와 나노시트 전극의 개발

Tran Le Luu[1]·Choonsoo Kim[2]·Jeyong Yoon[2*]
트란 루 레·김춘수·윤제용

[1]*Department of Mechatronics & Sensor Systems Technology, Vietnamese German University, Le Lai Street, Hoa Phu Ward, Thu Dau Mot City, Binh Duong Province, Viet Nam*
[2]*School of Chemical and Biological Engineering, College of Engineering, Institute of Chemical Process, Asian Institute for Energy, Environment & Sustainability (AIEES), Seoul National University (SNU), Gwanak-gu, Daehak-dong, Seoul 151-742, Korea*
[1]베트남 독일 대학교 메카트로닉스-센서 시스템 학과
[2]서울대학교 화학생물공학부 화학공정 신기술 연구소 & 아시아에너지환경지속가능발전 연구소

ABSTRACT

RuO_2 is a common active component of Dimensionally Stable Anodes (DSAs) for chlorine evolution that can be used in wastewater treatment systems. The recent improvement of chlorine evolution using nanostructures of RuO_2 electrodes to increase the treatment efficiency and reduce the energy consumption of this process has received much attention. In this study, RuO_2 nanorod and nanosheet electrodes were simply fabricated using the sol-gel method with organic surfactants as the templates. The obtained RuO_2 nanorod and nanosheet electrodes exhibit enhanced electrocatalytic activities for chlorine evolution possibly due to the active surface areas, especially the outer active surface areas, which are attributed to the increase in mass transfers compared with a conventional nanograin electrode. The electrocatalytic activities for chlorine evolution were increased up to 20 % in the case of the nanorod electrode and 35% in the case of the nanosheet electrode compared with the nanograin electrode. The RuO_2 nanorod 80 nm in length and 20-30 nm in width and the RuO_2 nanosheet 40-60 nm in length and 40 nm in width are formed on the surface of Ti substrates. These results support that the templated RuO_2 nanorod and nanosheet electrodes are promising anode materials for chlorine evolution in future applications.

Key words: Chlorine evolution, Electro-catalyst, nanorod, nanosheet, RuO_2

주제어: 전기화학촉매, 루테늄 옥사이드, 나노로드, 나노시트, 염소 발생, 염소발생 전극

1. Introduction

Chlorine is an essential product for the fields of chemical industry, pharmaceutical, and wastewater treatment (Schmittinger, 2000). Currently, an electrochemical process for generating chlorine is commonly used, and efficient anodes are necessary to meet industrial demands. Especially, dimensionally stable anodes (DSA) are popular as an

Received 25 July 2017, revised 1 September 2017, accepted 4 September 2017
*Corresponding author: Jeyong Yoon (E-mail: jeyong@snu.ac.kr)

electrocatalyst for chlorine evolution. This type of anode usually consists of a Ti support and noble metal oxide catalysts as either RuO_2, IrO_2 or their mixtures (Trasatti et al., 1984). In the case of the RuO_2 electrode, it has excellent electrocatalytic features for chlorine evolution such as low overpotential, low cost, enhanced selectivity, and mechanical and chemical stability (Tran et al., 2015). Roughly, 10-15% of the annual production of Ru goes into the fabrication of the DSAs (Srinivasan et al., 2006).

Although the electrolytic production of chlorine with the RuO_2 electrode is a well-established industrial process, a few drawbacks regarding the formation of unintended nanograins or nanoparticles have been reported (Gopiraman et al, 2013). Recently, to overcome these disadvantages, heterogenous nanostructure materials with favorable electrochemical properties have been investigated (Friedirich et al, 2009; Liu et al, 2011). Especially, one or two dimensional nanostructured materials of nanorods, nanowires, nanobelts, and nanosheets were reported to have unique properties such as a large active surface area, fast mass transfer, charge/discharge process, and high stability (Tiwari et al., 2012). However, these methods have a few limitations including using a lot of energy in the high temperature (1500˚C) vapor-phase processes and low yields.

Herein, we report the facile synthesis of RuO_2 nanorod and nanosheet electrodes with structures templated with PEG and SDS as surfactant assemblies. Contribution of the stabilizers such as sodium dodecyl sulfate (SDS) or polyethylene glycol (PEG) in the sol-gel process to achieve the desired shape is very important, and proposed as the basis of the surfactant inducing growth mechanism of nanomaterials in this study (Inoue et al., 1986; Li et al., 2003; Xia et al., 2003; Osmana et al., 2004; Dong and Jiao, 2006; Ananth et al., 2013).

The properties of these RuO_2 nanorod and nanosheet electrodes for chlorine evolution are compared with the conventional nanograin electrode. The microstructures of the as-prepared electrodes were evaluated with scanning electron microscopy (SEM), transmission electron microscopy (TEM) and X-Ray diffraction (XRD). The electrochemical properties were examined with cyclic voltammetry (CV), linear sweep voltammetry (LSV), and total chlorine concentration (DPD) methods.

2. Materials and Methods

2.1 Electrode preparation

The preparation of the titanium coated RuO_2 electrodes was done with the sol-gel method. This solution phase method, which is called sol-gel, can be carried out in soft-environments and appears to have positive effects on the fabrication of the RuO_2 electrode in terms of both a high electrocatalytic activity and stability in chlorine evolution (Panic et al., 1999; Panic et al., 2005; Osmana et al., 2008). Titanium foils (dimensions, $30 \times 20 \times 0.25$ mm, purity 99.7%, Aldrich-Sigma) were used as the substrate materials, for which the contaminants were removed by emery paper and then degreased in acetone. Then, they were etched in boiling concentrated hydrochloric acid at 86˚C for 1 h to produce a gray surface with uniform roughness. Three different methods were used to prepare the nanorods, nanosheets and conventional nanograins of the RuO_2 electrodes (Burrows et al., 1978; Kotz and Stuck, 1986). The nanorod structure was synthesized with SDS as the template. Ruthenium chloride, SDS, urea, and water were mixed at a molar ratio of 1:2:10:200 and stirred at 40˚C for 2 h to obtain a homogeneously mixed solution. Urea was used to gradually raise the pH value of the reaction mixture because heated urea above 60˚C is hydrolyzed to release ammonia, and then, precipitation occurred in the quiescent state. After a reaction time of 10 h, the mixture was immediately cooled to room temperature to prevent further hydrolysis of the urea. To fabricate the nanograin type electrode, 0.1 M $RuCl_3$ dissolved in 20 mL of de-ionized water was transferred into a two neck flat bottom flask and stirred with a magnetic stirrer. Twenty milliliters of 0.1 M NaOH were added drop wise over a course of 3 h. For the nanosheet structures, 0.4 g of PEG (dissolved in 20 mL of H_2O) were added to the nanograin recipe (0.1 M $RuCl_3$ + 0.1 M NaOH + 0.4 g PEG). The temperature of the solution was maintained at 75˚C for all the reactions. At the end

of each reaction, a black precipitate was formed. After discarding the supernatant, the precipitates were centrifuged, washed many times with de-ionized water to remove the unreacted chemicals, and then dried at 80°C for 5 h. Three milligrams of sol $Ru(OH)_x$ was dissolved in isopropanol and then coated onto the pretreated Ti substrates. Next, the electrodes were sintered at 450°C for 1 h to allow for hydrous removal and the formation of the metal oxides (Malmgren et al., 2010). One side of the electrode was covered with epoxy to prevent the exposure of the electrolytes.

2.2 Microstructure characterization

The microstructure and chemical compositions of the electrode surfaces were evaluated with field emission scanning electron microscopy (FE-SEM) coupled with an energy dispersive spectroscopy (EDS) system (JSM-6701F, JEOL Co., Japan). The SEM-EDS images were taken at a working distance of 7 mm with an accelerating voltage of 10 kV. The samples were positioned horizontally (Dong and Jiao, 2006). The EDS results confirmed an almost identical chemical composition of the three RuO_2 electrodes prepared. Each mass percentage of Ru loaded onto these electrodes is similar and suggests a fair comparison among the three electrode types: 31% for the nanorod electrode, 32% for the nanosheet electrode, and 32% for the nanograin electrode.

Crystal images were examined with a transmission electron microscope (TEM, JEOL 2000EXII, Japan). The TEM samples were prepared by scraping off the coating with a sharp knife and then dispersing the powders into isopropyl alcohol (Xia et al., 2003). A few drops of these solutions were deposited onto carbon film-coated Cu grids and analyzed with a microscope. The accelerating voltage was 110 kV; the vacuum system was 10 Pa, and the tilting angles were ± 25°.

To study the crystallinity of the RuO_2 electrodes, a high resolution X-ray diffraction pattern was obtained with the grazing incidence technique on a D8 Discover (Bruker-AXS, Germany) diffractometer (CuKα, λ = 1.5406 Å). A scintillation counter detector scanned between 25° and 100o in 2Θ; the angle of incidence was 0.5°; the working distance was 12 mm, and the accelerating voltage was 25 kV (Ananth et al., 2013).

2.3 Electrochemical measurements

The electrochemical characterizations of the as-prepared RuO_2 electrodes were done with cyclic voltammetry (CV, 0.5 M H_2SO_4) and linear sweep voltammetry (LSV) (Inoue et al., 2008). The experiments were performed at room temperature in a conventional single compartment cell with three electrodes using a computer-controlled potentiostat (PARSTAT 2273A, Princeton Applied Research, USA). The volume of the electrolyte solution in the cell was 150 ml. RuO_2 was used as the working electrode (anode), Pt (Samsung DSA, Korea) as the counter electrode (cathode), and Ag/AgCl (in saturated KCl) as the reference electrode (Kotz and Stuck, 1986).

The range of the scan rate was 5-320 mV/s. The CV curves were recorded at potentials ranging between 0-1 V. The voltammetric charge (q) obtained by the integration of the voltammetric curve is related with the number of electrochemically active surface areas, which are accessible by the electrolyte. The inner and outer surface areas were identified by plotting and extrapolating the voltammetric charges according to infinitely low (0) and fast (∞) scan rates, which was reported in previous studies (Klung, 1974; Burrows et al., 1978; Bard, 2001; Malmgren et al., 2010). The pseudo-capacitive reaction, which consists of coupled redox transitions involving proton exchange with the solution at a broad reversible peak around 0.6 V vs. Ag/AgCl, can be described as follows (Burrows et al., 1978; Bard, 2001):

$$RuO_x(OH)_y + zH^+ + ze^- \rightarrow RuO_{x-z}(OH)_{y+z} \quad (1)$$

LSV measurements were done in an electrolyte containing 5 M NaCl + 0.01 M HCl (pH 2) which is a favorable condition for chlorine evolution. The concentrations of the total active chlorine dissolved in the solution after the electrolysis in 0.1 M NaCl (pH 6) were determined by the DPD (N, N-diethyl-p-phenylenediamine) colorimetric method. The electrolysis time was 10 min., and the current

density was 16.7 mA cm^{-2}. In this method, DPD is oxidized to form a purple product, and the chlorine concentration was analyzed immediately with a spectrophotometer (DR/2010, HACH Co., Loveland, US) at 530 nm (Jeong et al., 2009). The chlorine concentrations were replicated three times, and their average values were reported.

3. Results and discussion

3.1 Surface analysis

3.1.1 Characteristics of the microstructure

Fig. 1 shows the SEM (a) and TEM (b) images of the RuO_2 electrodes with the different morphologies: nanorods, nanosheets, and conventional nanograins deposited onto the Ti substrates. As shown in Fig. 1 (a), the one dimensional nanorod structures grew almost in a random direction. The rods appear to be stable with a single layer and were separated from each other. On the other hand, the RuO_2 nanosheet electrode consists of hierarchical sheet nanostructures in an assembly of two dimensional subunits with a porous network and high interconnectivity. The nanosheet structures are perpendicular to the substrate and lead to a flower-like projected view with the sheet thickness approximately 10 nm. The formation of the pores is explained by the release of volatile gases such as H_2O and CO_2 during the heat treatment because of the decomposition of the precursor, in which organic additives were burnt up leaving behind porous structures. In contrast, the nanograin electrode consists of crystal RuO_2 nanoparticles with zero dimensions. The grains are finely agglomerated and appear to have a uniform size which is a characteristic trait of the sol-gel process. Overall, the RuO_2 nanorod and nanosheet electrodes have more open structures and roughness compared with the nanograin electrode. Clearly, the electrode morphologies are strongly influenced by the use of difference organic templates. The morphologies of the templated RuO_2 nanorod and nanosheet electrodes prepared by the sol-gel method were somewhat different with that prepared by reactive sputtering (Music et al., 2012; Chou et al., 2013; Zhao et al., 2014) or chemical vapor deposition methods (Han et al., 2010; Neupane et al., 2011; Lee et al., 2012), which are completely perpendicular and align to the substrate surfaces

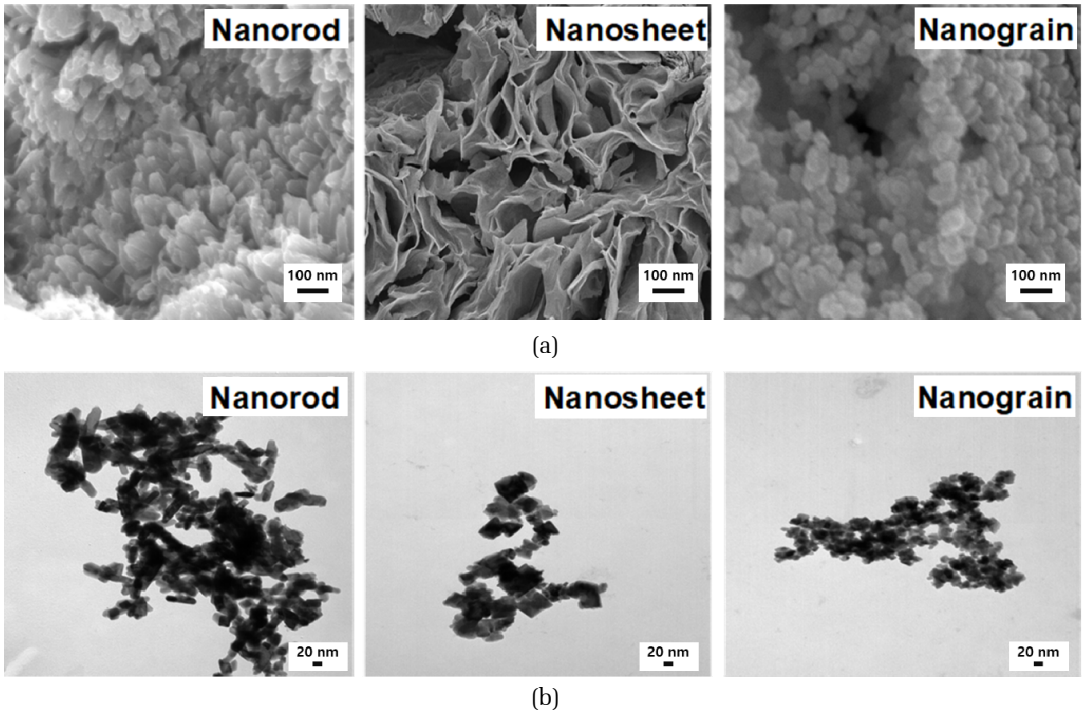

Fig. 1. SEM (a) and TEM (b) images of the RuO_2 nanorod, nanosheet, and nanograin electrodes.

The TEM images in Fig. 1 (b) show the different patterns of the RuO_2 nanorods, nanosheets, and nanograins, respectively. The nanorods present a core shape with a length of 80 nm and a width of 20-30 nm. The rods are polygonal prisms and continuous with a smooth surface, which may be due to the effect of the thermal treatment at 450˚C. Moreover, individual sheets about 40-60 nm in length and 40 nm in width are formed. The size of the nanosheets is uneven because of the controlled growth process resulting from the addition of the PEG. The total length and width of the RuO_2 nanorod and nanosheets show good crystallinities. On the other hand, the nanograins exhibit aggregated nanoparticles with a diameter size of about 20-30 nm. Undoubtedly, the organic template precursors have a crucial role in the shape evolution of the RuO_2 nanomaterials. These different morphologies are expected to influence the electrocatalytic efficiencies for chlorine evolution with the RuO_2 electrodes.

3.1.2 XRD spectra

Fig. 2 shows the diffraction patterns of the obtained RuO_2 electrodes with the different morphologies: nanorods, nanosheets and nanograins. There is little difference according to the crystal structures of these electrodes. The most pronounced peaks of RuO_2 were easily detected as follows: 110 and 101 planes at 28˚ and 35˚ in all of the electrodes. However, the peak for the 211 plane was very weak in the nanorod electrode, and the peak for the 310 plane did not exist in the nanorod and nanosheet electrodes. Nevertheless, all of these peaks for RuO_2 were observed in the nanograin electrode. It means that the nanograin electrode has a greater degree of polycrystallinity. The presence of sharp peaks for RuO_2 indicate the high purity and crystallinity of the as-synthesized RuO_2 nanostructures. The RuO_2 peaks reveal the formations of the rutile and solid phases, which are desirable in terms of electrode stability. The formation step of the RuO_2 metal oxide can be expressed as follows: the addition of NaOH or urea with $RuCl_3 \cdot xH_2O$ forms the precipitate of $Ru(OH)_3$ at the end of the reaction. $Ru(OH)_3$ is unstable and oxidizes in the presence of air during the initial heat treatment (100˚C drying process) which forms $RuO_2 \cdot nH_2O$ (Osmana et al., 2008).

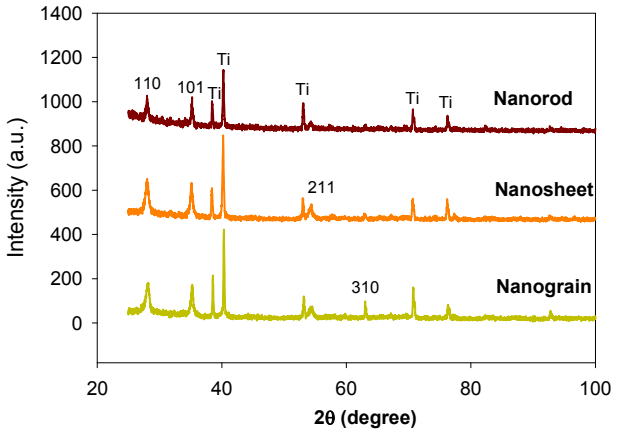

Fig. 2. XRD spectra of the RuO_2 electrodes with the different morphologies: nanorods, nanosheets, and nanograins.

Further heat treatment of the samples up to 450˚C causes the complete removal of water molecules and produces crystalline RuO_2. The catalyst layers are thin so that X-rays can penetrate through the coating layers, and the absorption peaks of the Ti metal can be realized. No evidence of the Ruthenium metallic phase by-product was observed, which can cause easy corrosion of components in chlorine electrolysis (Jeong et al., 2009).

3.2 Electrochemical properties

3.2.1 CV and active surface area

Fig. 3 shows the voltammetric charges at different scan rates (a) and the cyclic voltammograms at a scan rate of 4 mV/s (b) for the RuO_2 electrodes with the different morphologies: nanorods, nanosheets and nanograins. As shown in Fig. 3 (a), the voltammetric charge decreases with an increase in the scan rate, which is attributed to the difficulty of the electrolyte to penetrate into the inner surface of the electrode due to micropores, microcracks, and grain boundaries. Because the morphologies of the electrodes are different, the kinetics of the electrochemical reactions may vary according to the different areas of the electrode surface. At a fast scan rate, the protons do not have enough time to diffuse into the less accessible areas before the scan direction is reversed. At a low scan rate, the diffusion processes reach deeper into the oxide structure. The voltammetric charge is larger and decreases towards a constant value when the scan rate is increased.

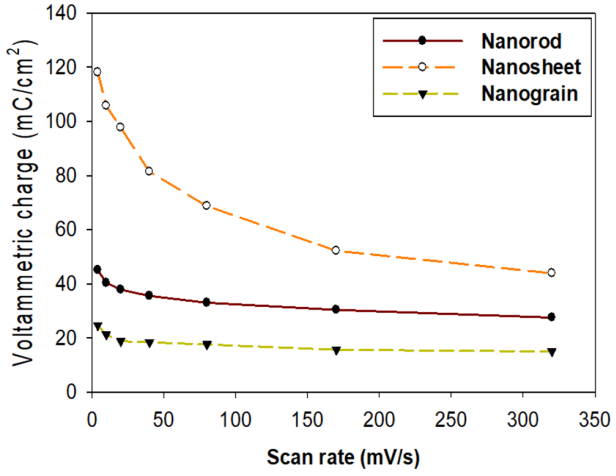

(a)

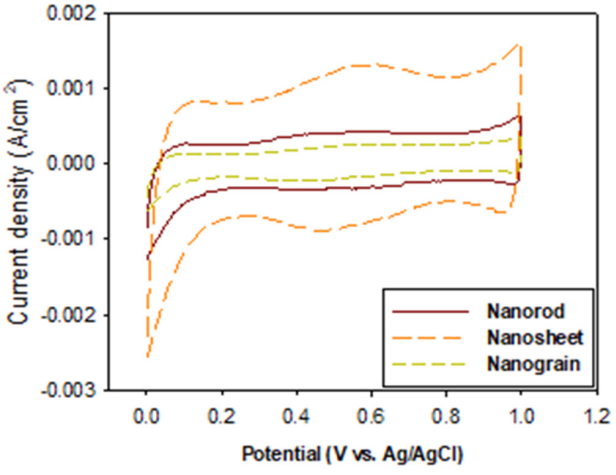

(b)

Fig. 3. Voltammetric charge with varying scan rates (a) and cyclic voltammetry at 4 mV/s (b) for the RuO_2 nanorod, nanosheet, and nanograin electrodes in H_2SO_4 (0.5 M).

The values of the voltammetric surface charges of the templated nanorod and nanosheet electrodes at both high and low scan rates are higher than that of the conventional nanograin electrode. The total voltammetric charges of the nanosheet and nanorod electrodes are 121.3 and 49.2 mC/cm^2 whereas that of the nanograin electrode is 28.8 mC/cm^2. The value of the outer voltammetric charges of these electrodes are 43.0, 27.5 and 15.1 mC/cm^2, respectively. Due to the characteristics of the RuO_2 nanorod and nanosheet electrodes such as highly open structures, high roughness factor and hierarchical pores with considerable interstices among them, the electrolyte easily accesses the inside of the rod or sheet structures for charge transport and ion diffusion compared to that of the conventional nanograin electrode. The nanosheet electrode shows the biggest gap between the total surface area and outer surface area, which could be attributed to the porous structure in the nanosheet which may provide a bigger inner surface area.

Fig. 3 (b) shows all the CV curves of the as-prepared electrodes. The CV curves of the RuO_2 electrodes showed rectangular shape. The redox proton exchange between the electrode and the acidic solution presents a broad reversible peak at 0.6 V vs. Ag/AgCl. The response current densities in the cyclic voltammograms for the nanorod and nanosheet electrodes are higher than those for the conventional nanograin electrode. Among these electrodes, the nanosheet electrode shows the highest response current density and electrochemical property.

3.2.2 Chlorine evolution efficiency

Fig. 4 shows the chlorine concentrations (a) and LSV (b) of the RuO_2 electrodes with the different morphologies: nanorods, nanosheets, and nanograins. As shown in Fig. 4 (a), there are differences in the chlorine evolution efficiencies of the as-prepared electrodes. The RuO_2 nanorod and nanosheet electrodes have higher chlorine concentrations than that of the conventional RuO_2 nanograin electrode. The chlorine evolution efficiency increases up to 35% and 20% in the case of the nanosheet (210 mg/L) and the nanorod electrodes (180 mg/L), respectively, compared with the conventional nanograin electrode (150 mg/L). At this chlorine measurement condition, oxygen evolution is suppressed by the increase of the oxygen overpotential and selectivity for chlorine evolution (Chen et al., 2012). The results of the chlorine concentrations are also supported by the LSV results in brine solution (5 M NaCl, 0.01 M HCl), which is shown in Fig. 4 (b). At potentials below 1.2 V vs. Ag/AgCl, no reaction takes place, but at potentials exceeding 1.2 V vs. Ag/AgCl, steady increase of current density was observed indicating chlorine formation. The steady state current of the nanorod and nanosheet electrodes appears to be more linear compared with the interrupt line of the nanograin electrode at 1.8 V, which can be affected by chlorine gas bubbles. Overall, the

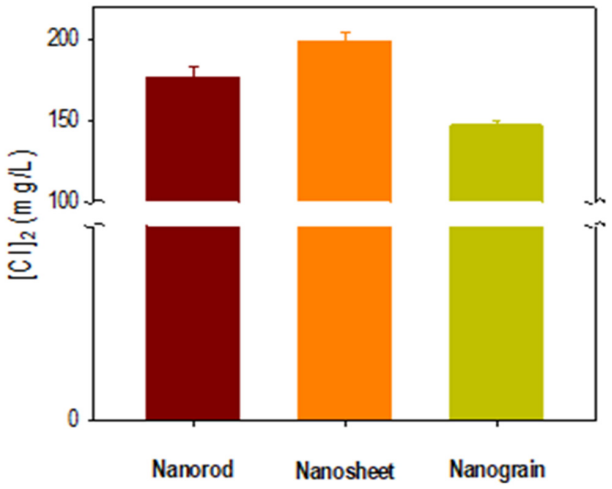

(a)

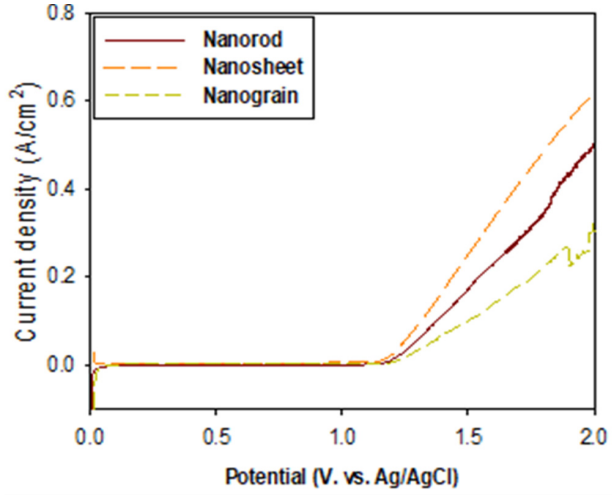

(b)

Fig. 4. Chlorine concentrations (a) and LSV (b) of the RuO_2 nanograin, nanorod, and nanosheet electrodes (0.1 M NaCl, pH 6, 16.7 mA/cm^2).

RuO_2 nanorod and nanosheet electrodes have a higher current density in the region of chlorine evolution compared with the nanograin electrode. This result implies that the nanorod and nanosheet RuO_2 electrodes possess higher chlorine electrocatalytic activities compared with the nanograin electrode. This result is explained by the higher outer surface areas of the nanorod and nanosheet electrodes. The outer surface area is the main working part for chlorine evolution because of the high reversibility and fast reaction, while the inner surface is blocked by adherent chlorine gas bubbles on the surface becoming partially inactive (Arizzone et al., 1990; Jeong et al., 2009; Chen et al., 2012). Undoubtedly, these nanorod and nanosheet structures do not only provide more outer electroactive sites which are effective electrolyte-accessible channels for ion transportation but also substantially improve the chlorine electrocatalytic performance.

4. Conclusions

This study showed that templated RuO_2 nanorod and nanosheet electrodes can be used as efficient electrocatalysts for chlorine evolution reactions when compared with that of the nanograin electrode. The RuO_2 nanorod and nanosheet electrodes were synthesized with a tailored architecture using organic templates and compared with the conventional nanograin electrode. The organic template precursors, the PEG or SDS surfactant, had a major role in controlling the morphology of the RuO_2 electrodes. The chlorine evolution efficiencies increased up to 20% and 35% in the case of the nanorod and nanosheet electrodes, respectively, compared with the nanograin electrode. These results are explained by the better mass transport of the RuO_2 nanorod and nanosheet electrodes due to more effective surface areas participating in the chlorine evolution reaction compared with that of the conventional nanograin electrode. This study supports that the templated RuO_2 nanorod and nanosheet electrodes are promising materials for higher electrocatalytic performance and the less energy consumption in the future chlor-alkali industry.

Acknowledgements

This research is supported by Korea Ministry of Environment as “Global Top Project (E617-00211-0608-0)" and a grant (code 17IFIP-B065893-05) from the Industrial Facilities & Infrastructure Research Program funded by the Ministry of Land, Infrastructure and Transport of Korea government.

References

A. Ananth, S. Dharaneedharan, M. Gandhi, M. Heo, Y. Mok (2013). Novel RuO_2 nanosheets – Facile synthesis, characterization and application, Chemical Chem. Eng. J. 223, 729–736.

A. Bard, L. Faulkner (2001). E*lectrochemical methods - Fundamentals and applications*, Wiley, New York, pp. 226-261

C. Malmgren, A. K. Eriksson, A. Cornell, J. Backtrom, S. Eriksson, H. Olin. (2010). Nanocrystallinity in RuO_2 coatings - Influence of precursor and preparation temperature, Thin Solid Films. 518, 3615-3618.

D. Music, J. Breunung, S. Mraz, J. Schneider (2012). Role of RuO_3 for the formation of RuO_2 nanorods, Appl. Phys. Lett. 100, 033108

G. Zhao, L. Zhang, K. Sun, H. Li (2014). Free-standing Pt@RuO_2·xH_2O nanorod arrays on Si wafers as electrodes for methanol electro-oxidation, J. Power Sources. 245, 892-897.

H. Friedrich, P. Jongh, A. Verkleij, K. Jong (2009). Electron tomography for heterogeneous catalysts and related nanostructured materials, Chem. Rev. 109, 1613-1626.

H. P. Klug, L. E. Alexander (1974). *X-ray Diffraction Procedures*, Wiley, New York.

J. Chou, Y. Chen, M. Yang, Y. Chen, C. Lai, H. Chiu, C. Lee, Y. Chueh, J. Gan (2013). RuO_2/MnO2 core–shell nanorods for supercapacitors, J. Mater. Chem. A. 1, 8753-8759.

J. Han, S. Lee, S. Kim, S. Han, C. Hwang, C. Dussarrat, and J. Gatineau (2010). Growth of RuO_2 thin films by pulsed-chemical vapor deposition using RuO4 precursor and 5% H_2 reduction gas, Chem. Mater. 22, 5700-5706.

J. Jeong, C. Kim, J. Yoon (2009). The effect of electrode material on the generation of oxidants and microbial inactivation in the electrochemical disinfection processes, Water Res. 43, p 895-901.

J. Osmana, J. Crayston, A. Pratt, D. Richens (2008). RuO_2–TiO_2 mixed oxides prepared from the hydrolysis of the metal alkoxides, Mater. Chem. Phys. 110, 256-262.

J. Tiwari, R. Tiwari, K. Kim, Zero-dimensional (2012). one-dimensional, two-dimensional and three-dimensional nanostructured materials for advanced electrochemical energy devices, Prog. Mater Sci. 57, 724-803.

L. Dong and J. Jiao (2006). Dielectrophoretic fabrication and electron microscopy characterization of one-dimensional-nanomaterial-based devices, Microscopy and Microanalysis. 12, 482-483.

M. CaO, Y. Wang, C. Guo, Y. Qi, C. Hu, E. Wang (2004). A simple route towards CuO nanowires and nanorods, J. Nanosci. Nanotechnol. 4, 824-828.

M. Gopiraman, S. Babu, Z. Khatri, K. Wei, M. Endo, R. Karvembu and I. Kim (2013). Facile and homogeneous decoration of RuO_2 nanorods on graphene nanoplatelets for transfer hydrogenation of carbonyl compounds, Catal. Sci. Technol. 3, 1485.

P. Schmittinger (2000). *Chlorine: principle and industrial practice*, Wiley, New York, 21-34.

R. Burrows, D. Denton and J. Harrision (1978). Chlorine and oxygen evolution on various compositions of RuO_2/TiO_2 electrodes, Electrochim. Acta. 23, 493-500.

R. Chen, V Trieu, A. R. Zeradjanin, H. Natter, D. Teschner, J. Kintrup, A. Bulan, W. Schuhmann and R. Hempelmann (2012). Microstructural impact of anodic coatings on the electrochemical chlorine evolution reaction, Phys. Chem. Chem. Phys. 14, 7392-7399.

R. Chen, V. Trieu, H. Natter, J. Kintrup, A. Bulan, R. Hempelmann (2012). Wavelet analysis of chlorine bubble evolution on electrodes with different surface morphologies, Electrochem. Commun. 22, 16-20.

R. Liu, J. Duay and S. Lee (2011). Heterogeneous nanostructured electrode materials for electrochemical energy storage, Chem. Commun. 47, 1384-1404.

R. Kotz and S. Stuck (1986). Stabilization of RuO_2 by IrO_2 for anodic oxygen evolution in acid media, Electrochim. Acta. 31, 1311-1316.

S. Ardizzone, G. Fregonara, S. Trasatti (1990). Inner and outer active surface of RuO_2 electrodes, Electrochim. Acta. 35, 263-267.

S. Neupane, G. Kaganas, R. Valenzuela, L. Kumari, X. Wang, W. Li. (2011). Synthesis and characterization of ruthenium dioxide nanostructures, J. Mater Sci. 46, 4803-4811.

S. Trasatti (1984) Electrocatalysis in the anodic evolution of oxygen and chlorine, Electrochim. Acta. 29, 1503-1512.

Tran Le Luu, Jiye Kim, Jeyong Yoon (2015). hysicochemical properties of RuO_2 and IrO_2 electrodes affecting chlorine evolutions, Journal of J. Ind. Eng. Chem. vol 21, 400-404.

V. Panic, A. Dekanski, S. Milonjic, R. Atanasoski, B. Nikolic (1999). RuO_2–TiO_2 coated titanium anodes obtained by the sol–gel procedure and their electrochemical behaviour in the chlorine evolution reaction, Colloids

Colloids Surf. A. 157, 269-274.
V. Panic, A. Dekanski, M. Stankovic, S. Milonjic, B. Nikoli (2005). On the deactivation mechanisms of RuO_2–TiO_2/Ti anodes prepared by the sol–gel procedure, J. Electroanal. Chem. 579, 67-76.
V. Srinivasan, P. Arora, P. Ramadass (2006). Report on the electrolytic industries for the year 2004, Journal of the J. Electrochem. Soc. 153, K1.
V. Trieu, B. Schleya, H. Nattera, J. Kintrup, A. Bulan (2012). R. Hempelmann, RuO_2-based anodes with tailored surface morphology for improved chlorine electro-activity, Electrochim. Acta. 78, 188-194.
Y. Inoue, M. Uota, M. Uchigasaki, S. Nishi, T. Torikai, T. Watari, M. Yada (2008). Helical Ruthenium compound templated by 1-Dodecanesulfonate assemblies and its conversion into helical Ruthenium oxide and helical metallic Ruthenium, Chem. Mater. 20, 5652-5656.
Y. Lee, B. Kim, H. Jung, J. Shim, Y. Lee, C. Lee, J. Baik, W. Kim, M. Kim (2012). Hierarchically grown single crystalline RuO_2 nanorods on vertically aligned few walled carbon nanotubes, Mater. Lett. 89, 115-117.
Y. Xia, P. Yang, Y. Sun, Y. Wu, B. Mayers, B. Gates, Y. Yin, F. Kim, H. Yan (2003). One dimensional nanostructures: synthesis, characterization, and applications, Adv. Mater. 15, 353-389.
Z. Li, Y. Xiong, Y. Xie (2003). Selected-control synthesis of ZnO nanowires and nanorods via a PEG-assisted route, Inorg. Chem. 42, 8105-8109.

SUPPORTING INFORMATION

Calculation of the total and outer surface areas

The voltammetric charge q dependent on the applied potential scan rate is used to extrapolate the surface area. At a low scan rate, the whole surface with the inner and outer surface can exchange protons with the solution whereas at a fast scan rate, the penetration of the protons becomes the rate determining step, and only the outer surface contributes to this reaction (Klug and Alexander, 1974; Burrows et al., 1978; Malmgren et al., 2010; Bard, 2001). This might be related to the existence of less accessible surface regions, like pores and cracks, which progressively do not participate in the reaction as the scan rate is increased. Hence, by plotting and extrapolating the surface area according to infinitely low (0) and fast (∞) scan rates, it is possible to separate the inner and outer surface. The following equations are used (Burrows et al., 1978):

$$q_{total} = q_{inner} + q_{outer} \quad (s1)$$

$$q(\nu) = q_{outer} + A(1/\sqrt{\nu}) \quad (s2)$$

$$1/q(\nu) = 1/q + B\sqrt{\nu} \quad (s3)$$

where v is the scan rate; $q(\nu)$ is the voltammetric charge at the scan rate ν; qtotal is the voltammetric charge obtained at an infinitely low (0) scan rate; q_{outer} is the voltammetric charge obtained at a high (∞) scan rate; q_{inner} is related to the voltammetric charge of the inner surfaces, and A and B are constants.